

Article

Assessing the Spatial Benefits of Green Roofs to Mitigate Urban Heat Island Effects in a Semi-Arid City: A Case Study in Granada, Spain

Francisco Sánchez-Cordero ^{1,*}, Leonardo Nanía ¹, David Hidalgo-García ² and Sergio Ricardo López-Chacón ³

- ¹ Department of Structural Mechanics and Hydraulic Engineering, Universidad de Granada, 18071 Granada, Spain; lnania@ugr.es
² Technical Superior School of Building Engineering, Universidad de Granada, 18071 Granada, Spain; dhidalgo@ugr.es
³ Departament d'Enginyeria Civil i Ambiental, Universitat Politècnica de Catalunya (UPC Barcelona-Tech), 08034 Barcelona, Spain; sergio.ricardo.lopez@upc.edu
* Correspondence: f.sanchezcordero@ugr.es

Abstract: Studies show that Nature-Based Solutions can mitigate Urban Heat Island (UHI) effects by implementing green spaces. Green roofs (GRs) may minimize land surface temperature (LST) by modifying albedo. This research predicts, assesses, and measures the impact of reducing the LST by applying green roofs in buildings by using a Random Forest algorithm and different remote sensing methods. To this aim, the city of Granada, Spain, was used as a case study. The city is classified into different Local Climate Zones (LCZs) to determine the area available for retrofitting GRs in built-up areas. A total of 14 Surface Temperature Collection 2 Level-2 images were acquired through Landsat 8–9, while 14 images for spectral indices such as the Normalized Difference Vegetation Index (NDVI), the Normalized Difference Building Index (NDBI), and Proportion Vegetation (PV) were calculated from Sentinel-2 in dates coinciding or close to LST images. Additional factors were considered including the sky view factor (SVF) and water distance (WD). The results suggest that Granada has limited suitable areas for retrofitting GRs, and available areas can reduce LST with a moderate impact, at an average of 1.45 °C; however, vegetation plays an important role in decreasing LST. This study provides a methodological example to identify the benefits of implementing GRs in reducing LST in semi-arid cities and recommends a combination of strategies for LST mitigation.



Academic Editor: Hua Liu

Received: 31 March 2025

Revised: 5 June 2025

Accepted: 11 June 2025

Published: 16 June 2025

Citation: Sánchez-Cordero, F.; Nanía, L.; Hidalgo-García, D.; López-Chacón, S.R. Assessing the Spatial Benefits of Green Roofs to Mitigate Urban Heat Island Effects in a Semi-Arid City: A Case Study in Granada, Spain. *Remote Sens.* **2025**, *17*, 2073. <https://doi.org/10.3390/rs17122073>

Copyright: © 2025 by the authors. Licensee MDPI, Basel, Switzerland. This article is an open access article distributed under the terms and conditions of the Creative Commons Attribution (CC BY) license (<https://creativecommons.org/licenses/by/4.0/>).

Keywords: urban heat island; land surface temperature; green roof; random forest; local climate zone; machine learning

1. Introduction

The continuous increase in greenhouse emissions contributes to global warming and leads to more frequent extreme weather events such as droughts, heatwaves, and floods [1–3]. It is estimated that 30% of the world's population experiences extreme heat conditions, and forecasts indicate that this will reach 74% in the next 20 years [4]. In cities, the ongoing development and rapid growth of new buildings prioritize construction zones over the expansion of green vegetated areas. This prioritization increases the absorption of solar heat and reduces solar reflectivity (albedo) [5], leading to larger areas of cities that are vulnerable to thermal discomfort and rising temperatures. As a result, residents may face health risks associated with high urban temperatures. Nowadays, it is extremely important

that city planning is carried out for a healthy urban environment. For understanding thermal comfort in urban areas, the Urban Heat Island (UHI) phenomenon is widely used in the literature [6–10]. The UHI is defined as the difference in the temperature between urban and surrounding rural areas induced by replacing the natural land surface with the urban fabric [11]. The effect of the UHI occurs when an increased heat flux from the land surface is moved into the atmosphere near cities [12]. Furthermore, UHI effects are notably amplified in extreme events like heat waves, which synergize and aggravate thermal comfort [13–18]. This scenario poses a significant dilemma, as the expansion of urban areas is the main driver of the economy but alters local urban climate by increasing land surface temperature [19,20].

In the Mediterranean, future heat waves are projected to increase significantly. In Spain, a more frequent occurrence of heatwaves has been observed since the early 1980s, characterized by an increase in the number of events, their duration, and intensity [1,21,22]. In this sense, cities experience the greatest temperature increases exacerbated by the UHI phenomenon and environmental pollution from the transportation and industrial sectors [23]. Despite weather stations and on-site methods providing data to comprehend the rise in urban air temperatures, these methods often yield insufficient data for larger area expansions. In this sense, advances in remote sensing techniques have become valuable. Satellite images obtained through thermal infrared sensors allow for studies of Land Surface Temperature (LST) and have been found to be consistent as a proxy for air temperature [24], enabling the identification of Surface Urban Heat Islands (SUHI) by directly evaluating land surface temperatures (LST) [13].

In recent years, several mitigation measures have been researched and developed to reduce urban temperatures. However, the possibility of implementing large-scale UHI mitigation activities differs from one location to another. Zhao et al. [6] and Berardi et al. [25] summarized measures at building and neighborhood scales. Among these are solutions for changing construction materials to modify albedo, making it more reflective; for instance, cool pavements [26], reflective roofs, cool surfaces [27], evaporative pavements, thermally efficient buildings, constructed shade, and Nature-Based Solutions (NBS) [28,29]. The latter is dedicated to restoring and collaborating with nature in urban areas. Amid Nature-Based Solutions are urban greenery, green roofs (GRs), and green walls [30–32]. The advantage of vegetation, apart from shade provision and increased albedo, is evapotranspiration. It is a key physical process that transfers some of the surface heat flux into latent heat, which is then released into the external environment, reducing air temperature [33,34]. These green areas were conceived to mitigate temperatures and the urban heat island effect [35,36], reduce levels of environmental pollution [37–44], achieve energy savings by improving thermal insulation [45–48] and promoting ecological biodiversity in urban areas [49,50]. Thus, strategic locations might contribute to diminishing UHI [51]. These are some benefits that could lead to an enhancement in the well-being of inhabitants.

In urban areas, green spaces play an important role in diminishing temperature to improve the thermal environment [52], and green solutions are the fastest and easiest way to reduce and adjust a city's heat and temperature [15]. A study by Nastran et al. [53] examined the relationship between the UHI and urban green spaces on European cities. They found that in Mediterranean cities, a high proportion of forested areas is linked to lower temperatures. Additionally, Marando et al. [54] emphasized that almost one-third of functional European urban areas have tree cover below 16%, recommending rapid implementation of green infrastructure to mitigate UHI effects.

Machine learning methods have shown remarkable potential to deal with nonlinear correlation patterns that help us understand the relationship between urban features and LST [55–57]. Consequently, they constitute a useful tool to describe the effect of vegetation

on LST variation. According to the literature, the NDVI has been shown to have a negative correlation with LST, while the NDBI exhibits a positive correlation with LST [58].

Considering the exposed advantages of green urban recovery, the goal is to decrease the high values of the NDBI linked to built-up areas, which are positively correlated with LST, by increasing greenness. This study aims to evaluate the benefits of installing GRs in a semi-arid climate city like Granada, Spain, by predicting LST using a machine learning method. Therefore, a non-parametric model such as Random Forest (RF) is selected. The objective is to assess how these greening installations can enhance resilience to rising temperatures affecting the quality of life for residents in Mediterranean urban areas suffering from increasing UHI effects. The research will tackle the following key questions:

- Which built-up LCZs are more impacted by higher LST in Granada?
- Is the city suitable for implementing GRs to minimize heat temperatures?
- What is the impact on LST of implementing extensive GRs?

2. Materials and Methods

2.1. Study Area

The city of Granada, located in the south of Spain (Figure 1), is classified as climate type Csa according to the Köppen–Geiger climate classification, indicating a Mediterranean zone with hot and dry summers and wet and cold winters [59]. The average temperature fluctuates between 6.50 °C in January and 32 °C in July, with minimums in winter of −3.0 °C and extremes in summer of 45 °C. Spain has experienced more frequent heatwave occurrences, and Granada suffers more than two mean annual events [22]. Therefore, it is a suitable choice for conducting this study. The study research area covered about 27.90 km² (projection: ETRS89/UTM zone 30N—CRS 25830).

2.2. Methodology

To comprehend LST variation in urban areas during summer in Granada, the following procedure was implemented. First, a Local Climate Zone (LCZ) map was obtained to distinguish between different built and land cover types across the study area. This classification has significantly contributed to the scientific community's better understanding of the urban climate [60].

Second, 14 LST images were derived from Landsat 8–9 for the summer months of July and August in the years 2022, 2023, and 2024, while 14 urban parameters—the NDVI, PV, NDBI, and Normalized Difference Water Index (NDWI)—were calculated from Sentinel-2.

Third, a Normalized Digital Surface Model (nDSM) was generated from LiDAR points to locate potential areas for GR retrofitting. Other key parameters, including the SVF and WD, were obtained to improve LST estimation.

Finally, a Random Forest algorithm was employed to assess the relationship between LST and all the parameters. Subsequently, NDVI, NDBI, and PV values were altered in potential areas for GRs. The main objective is to assess the temperature reduction by predicting LST using GRs after identifying available areas to retrofit GRs as a solution. The methodology is summarized in Figure 2.

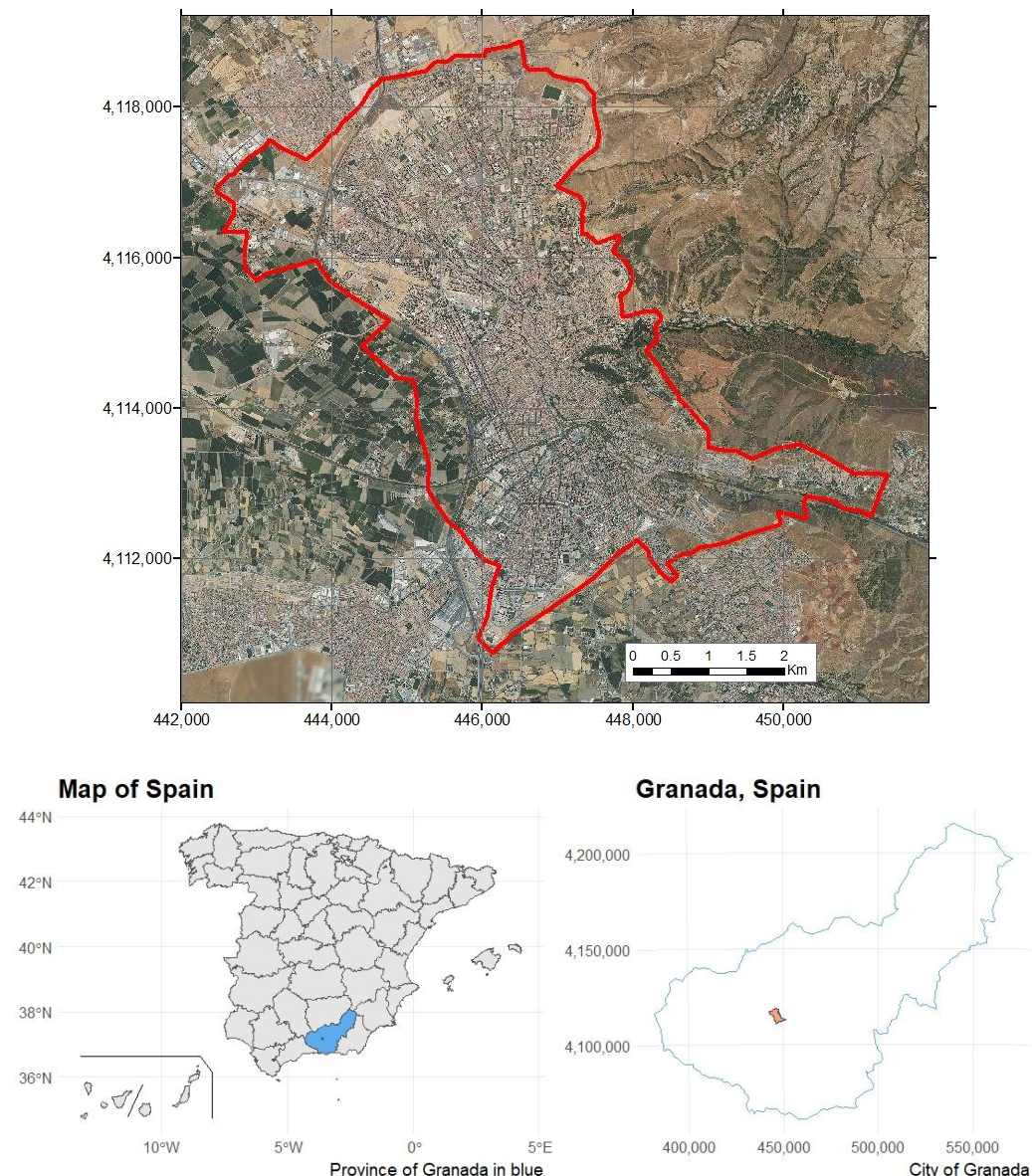


Figure 1. Map of Granada, Spain.

2.3. Map and LCZ Classification

The Local Climate Zone (LCZ) classification was originally proposed by authors Steward and Oke in 2012 [61]. Since then, the mapping methods developed have been based on remote sensing, GISs, and combined techniques. The LCZ classification has gained extraordinary growth due to the use of the LCZ Generator Tool. This platform uses a Random Forest algorithm for LCZ classification and has continuously implemented a variety of deep learning models since 2017 [60].

Our purpose is to study the possible thermal characteristics among different LCZ types. Previous studies have successfully employed LCZ classification to assess urban thermal environments, yielding notable results [62,63].

We generated the LCZ map for Granada using the LCZ Generator [64]. It features 14 standard LCZ classes, explained in Figure 3. According to the LCZ Generator, the overall accuracy value is 0.47, with a weighted accuracy of 0.86.

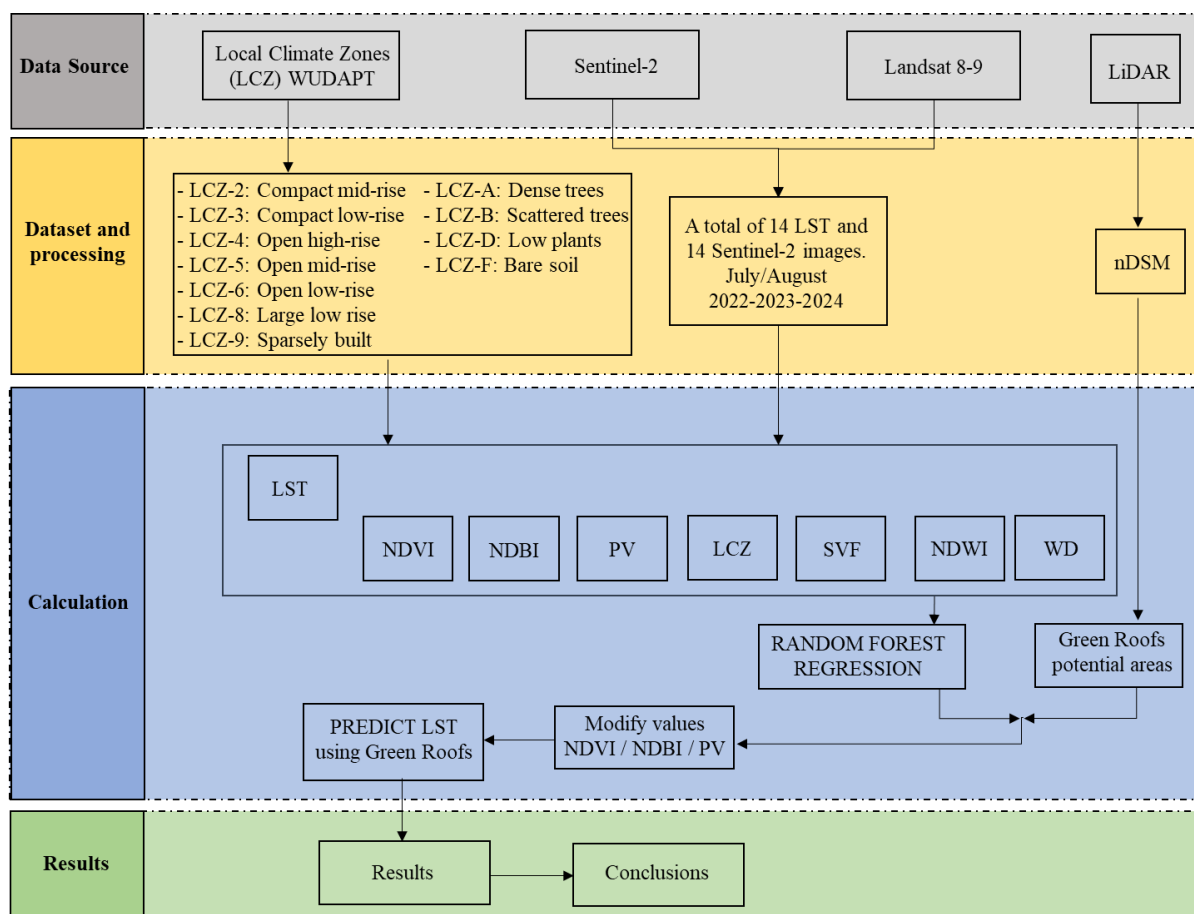


Figure 2. Methodology scheme. The Random Forest model is used to predict changes in land surface temperature resulting from the implementation of green roofs, by modifying NDVI, NDBI, and PV.

The LCZ map for Granada is depicted in Figure 4. Notably, the urban areas primarily consist of zone types, including LCZ-2 (compact midrise), LCZ-3 (compact low-rise), LCZ-5 (open midrise), LCZ-6 (open low-rise), LCZ-8 (large low-rise), and LCZ-9 (sparsely built), covering 71.70% of the total surface. Conversely, rural zones or land cover types contain natural coverage types such as LCZ-A, B, C, D, and F, comprising 28.30%. Figure 5 illustrates the urban spatial percentage containing each LCZ within the study area. LCZs 2, 5, and D exhibit the largest extents, while LCZs E, 9, and F are the least extensive. In the southeast region, mixed patterns between LCZ-A, B, C, and D are found. Meanwhile, LCZ-1 (compact high-rise) was not considered due to being under-represented or nonexistent in the study area.

2.4. Landsat 8–9 LST Retrieval

A total of 14 Landsat 8–9 Collection-2 Level 2 science products (L2SP) [65] were acquired to derive Surface Temperature data (Path 200 Row 034) for the summer months of July and August in the years 2022, 2023, and 2024. The acquired images are categorized as Tier 1 with cloud coverage lower than 15%. The LST images provide a 30 m spatial resolution, correspond to daytime hours, at 10:49 AM, and were converted to degrees in Celsius (°C) for the analysis.

The LST values in Granada range from a minimum of 32.5 °C to a maximum of 62.2 °C, with a mean value of 46 °C.

BUILT TYPES (URBAN)	DEFINITION	LAND COVER TYPES (NATURAL)	DEFINITION
LCZ-1 COMPACT HIGHRISE	Dense mix of tall buildings to tens of stories. Buildings closely spaced. Sky view from street level significantly reduced. Land cover mostly paved; few or no trees. High space heating/cooling demand. Heavy traffic flow.	LCZ-A DENSE TREES	Heavily wooded landscape. Land cover mostly pervious (low plants). F is natural forest, tree cultivation, or urban park.
LCZ-2 COMPACT MIDRISE	Dense mix of midrise buildings. Few or no trees. Land cover mostly paved. Stone, brick, tile, and concrete construction materials.	LCZ-B SCATTERED TREES	Lightly wooded landscape. Land cover mostly pervious (low plants). F is natural forest, tree cultivation, or urban park.
LCZ-3 COMPACT LOW-RISE	Dense mix of low-rise buildings. Few or no trees. Land cover mostly paved. Stone, brick, tile, and concrete construction materials.	LCZ-C BUSH, SCRUB	Open arrangement of bushes, shrubs, and short, woody trees. Land cover mostly pervious (bare soil or sand). F is natural scrubland or agriculture.
LCZ-4 OPEN HIGH-RISE	Open arrangement of tall buildings to tens of stories. Abundance of pervious land cover (low plants, scattered trees).	LCZ-D LOW PLANTS	Landscape of grass or herbaceous plants/crops. Few or no trees. F is natural grassland, agriculture, or urban park.
LCZ-5 OPEN MIDRISE	Open arrangement of midrise buildings. Abundance of pervious land cover (low plants, scattered trees).	LCZ-E BARE ROCK OR PAVED	Landscape of rock or paved cover. Few or no trees or plants. Zone function is natural desert (rock) or urban transportation.
LCZ-6 OPEN LOW-RISE	Open arrangement of low-rise buildings. Abundance of pervious land cover (low plants, scattered trees).	LCZ-F BARE SOIL OR SAND	Landscape of soil or sand cover. Few or no trees or plants. Zone function is natural desert or agriculture.
LCZ-8 LARGE LOW-RISE	Open arrangement of large low-rise buildings. Few or no trees. Land cover mostly paved.		
LCZ-9 SPARSELY BUILT	Sparse arrangement of small or medium-sized buildings in a natural setting. Abundance of pervious land cover (low plants, scattered trees).		

Figure 3. Local Climate Zone types and definitions. Image adapted from Stewart and Oke [61].

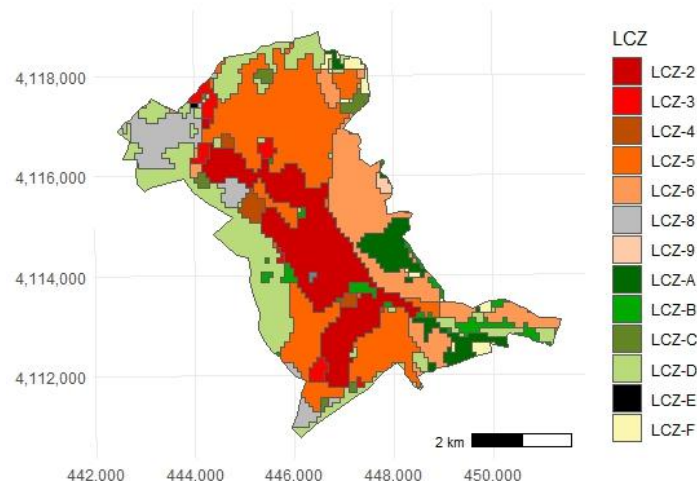


Figure 4. Local Climate Zones for Granada, Spain. Source: LCZ Generator.

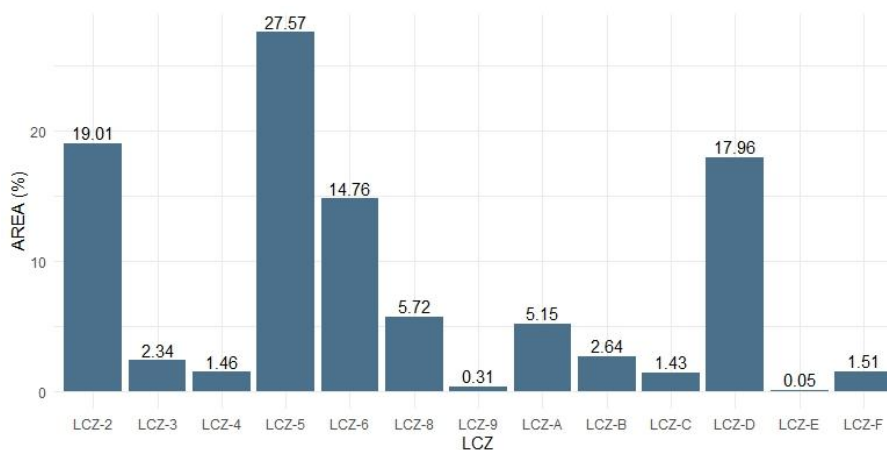


Figure 5. The percentage of coverage of different Local Climate Zones (LCZ) in Granada.

2.5. Sentinel-2 Images and Spectral Indices Used

Sentinel-2 satellites provide images of the Earth's surface, with resolutions ranging from 10 to 60 m. For this research, 14 Level-2A products were selected based on dates that were close to or the same as those of the Landsat image, all corresponding to daytime hours at 10:56 AM. The spectral indices NDVI, NDBI, NDWI, and PV were calculated. Data was obtained from a cloud cover index of less than 15% and a resolution of 10 m. The equations for the different spectral indices determined using Sentinel-2 data are presented in Table 1.

Table 1. Derivation of spectral indices using Sentinel-2 imagery.

Index	Equation	Number	Reference
NDVI	$NDVI = \frac{NIR - Red}{NIR + Red}$	(1)	[19]
PV	$PV = \left[\frac{NDVI - NDVI_{min}}{NDVI_{max} - NDVI_{min}} \right]^2$	(2)	[66]
NDBI	$NDBI = \frac{SWIR_1 - NIR}{SWIR_1 + NIR}$	(3)	[67]
NDWI	$NDWI = \frac{Green - NIR}{Green + NIR}$	(4)	[68]

The NDVI estimates the health and condition of vegetation, with values ranging from -1 to 1 , while the PV index represents the vegetation fraction. It estimates the proportion of an area covered by vegetation, ranging from 0 (bare soil) to 1 (vegetation). In Equation (1), the NDVI is calculated using the optical bands of the near-infrared (NIR) and red bands (Red). In Equation (2), the NDVI max and NDVI min are the maximum and minimum values of the NDVI interval calculated using Equation (1).

The NDBI identifies and quantifies urbanized or built-up areas, with values ranging from -1 to 1 , consequently providing insight into urban expansion and city monitoring. To calculate the NDBI, short-wave infrared (SWIR) and NIR bands are used, according to Equation (3). Furthermore, the NDWI is calculated using Equation (4) to extract water information, allowing the detection of water bodies. The results for each spectral index are depicted in Figure 6. A summary of the dates from Sentinel-2 and Landsat 8–9 images for this study is provided in the Table 2.

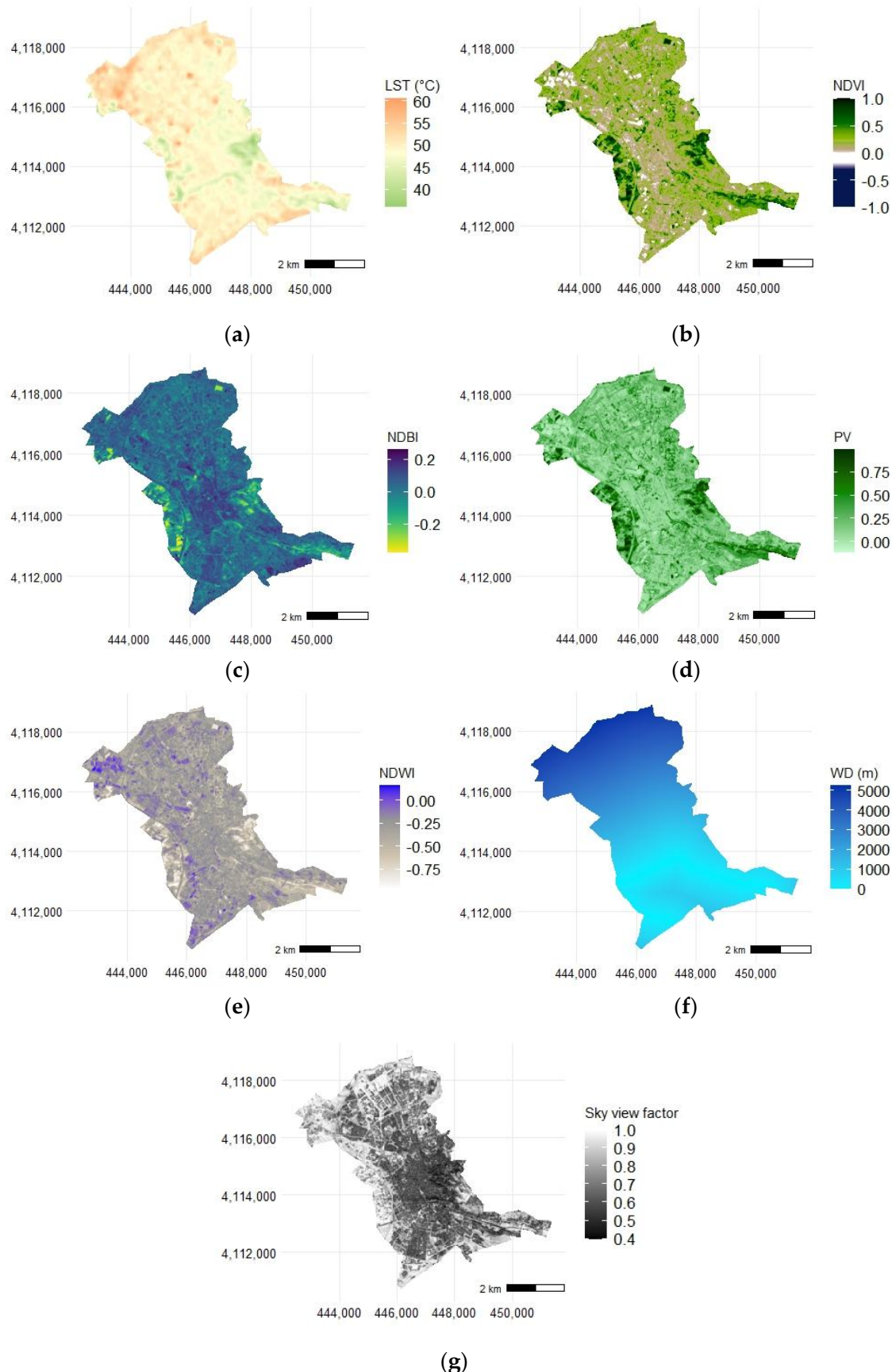


Figure 6. Raster visualizations of key surface parameters: (a) LST, (b) NDVI, (c) NDBI, (d) PV, (e) NDWI, (f) WD, and (g) SVF.

Table 2. Landsat surface temperature and Sentinel-2 image retrieval dates.

LST	Landsat ID	LST Date	Sentinel ID	Sentinel Date
1	LC09	11 July 2022	S2A	12 July 2022
2	LC08	19 July 2022	S2A	22 July 2022
3	LC09	27 July 2022	S2B	27 July 2022
4	LC08	4 August 2022	S2B	6 August 2022
5	LC09	28 August 2022	S2B	26 August 2022
6	LC09	30 July 2023	S2A	27 July 2023
7	LC08	7 August 2023	S2A	6 August 2023
8	LC08	23 August 2023	S2B	21 August 2023
9	LC08	8 July 2024	S2A	11 July 2024
10	LC09	16 July 2024	S2B	16 July 2024
11	LC09	1 August 2024	S2A	5 August 2024
12	LC08	9 August 2024	S2A	10 August 2024
13	LC09	17 August 2024	S2A	20 August 2024
14	LC08	25 August 2024	S2B	25 August 2024

LC09 = Landsat 9, LC08 = Landsat 8, S2A = Sentinel-2A, S2B = Sentinel-2B.

2.6. Estimation of Parameters Sky View Factor and Water Distance

The sky view factor (SVF) measures the ratio of radiation received or emitted by a flat surface to that of the surrounding hemispherical environment, reflecting how much of the sky is visible from that surface. It is a dimensionless parameter with values ranging from 0 to 1, where values close to 0 represent limited sky visibility, while 1 represents a completely visible sky. This parameter was obtained from the DSM and the UMEP tool (version 4.1.1) [69] in QGIS; then, it was resampled to 30 m to coincide with LST raster. Water distance (WD) was calculated using river shapefiles and comparing with google earth photos to locate water bodies and set the target pixels to create a raster proximity map.

2.7. Surface Temperature Mitigation

The hypothesis of this study is that green roofs (GRs) are effective in reducing land surface temperature (LST). For descriptive analysis, surface temperatures of two different roofs on the same building in Granada were obtained using a thermal imagery camera (FLIR E8). One roof is a traditional roof located on the third floor, while the other roof, located on the second floor, is covered with a GR over an area of approximately 380 m². Both roofs have the same orientation.

Thermal imagery provided evidence of surface temperature reductions on two different roofs of the same building on 6 July 2023 and 1 July 2024. For example, the conventional roof can easily reach values of 36 °C (Figure 7a). In contrast, the implementation of a green roof results in significant temperature reductions in areas with scarce vegetation and dense vegetation coverage, recording temperatures of 29 °C and 25 °C, respectively (Figure 7b). This is consistent with previous studies that emphasize the importance of maintaining dense vegetation coverage because plants have a higher albedo than the substrate [12,48,70,71]. Our objective is to further investigate the effects of green roofs on the city scale.

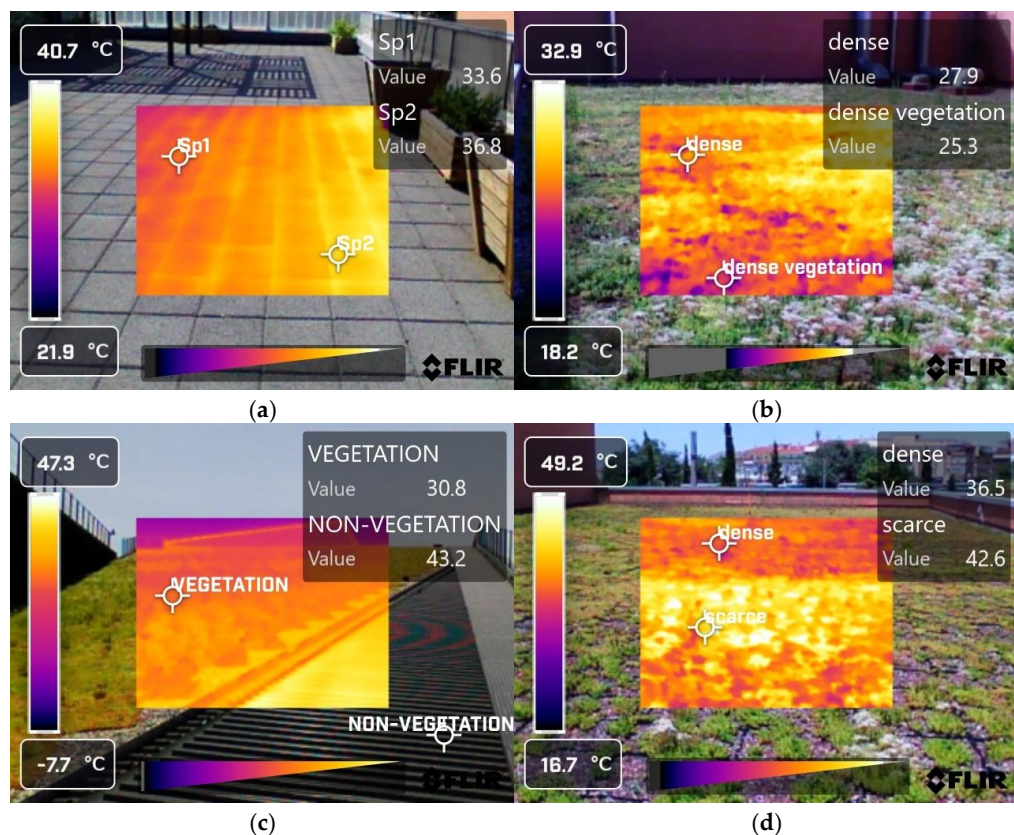


Figure 7. Examples of thermal imagery. (a) Surface temperature of a conventional roof; (b) surface temperature of a green roof; (c) mixed roofing surfaces; (d) comparison between areas with scarce and dense vegetation.

2.8. Green Roof Areas Selection Criteria

For city planning, remote sensing is essential for defining urban structure types and characterizing the morphology of cities [72]. LiDAR helps understand a city in 3D, identifying buildings and vegetation height. In this sense, GR selection criteria for Granada were obtained beginning with LiDAR point clouds from the Spanish National Orthophoto Program (PNOA) with a density of 1.5 points/m². Point data was processed using the R package *lidR* (version 4.1.2) [73] and consequently generating a Digital Terrain Model (DTM) and DSM, as depicted in Figure 8a,b. To obtain building heights, the DSM was subtracted from the DTM, obtaining the nDSM as shown in Figure 8c [74]. For visualization purposes, Figure 8 illustrates just a part of the study area, not the entire delimited zone. Areas capable of implementing GRs are evaluated according to the following conditions:

- Firstly, the slope is obtained in QGIS from the nDSM raster.
- Secondly, only pixels with a slope below 15% are considered from the slope raster. This threshold was chosen for practical reasons, such as stormwater management. Slope is an important factor because lower slopes enhance the GR stormwater retention and detention capacity [75,76], avoid drying out faster, and reduce erosion problems. Additionally, lower slopes allow for the installation of photovoltaic panels, which have gained popularity recently for their ability to provide combined benefits [77].
- Thirdly, these pixels were joined and converted to shapefiles. Areas smaller than 50 m² were excluded, as they were deemed too small to have a significant impact. The selected areas are depicted in Figure 8d and represent actual roof areas suitable for roof greening.

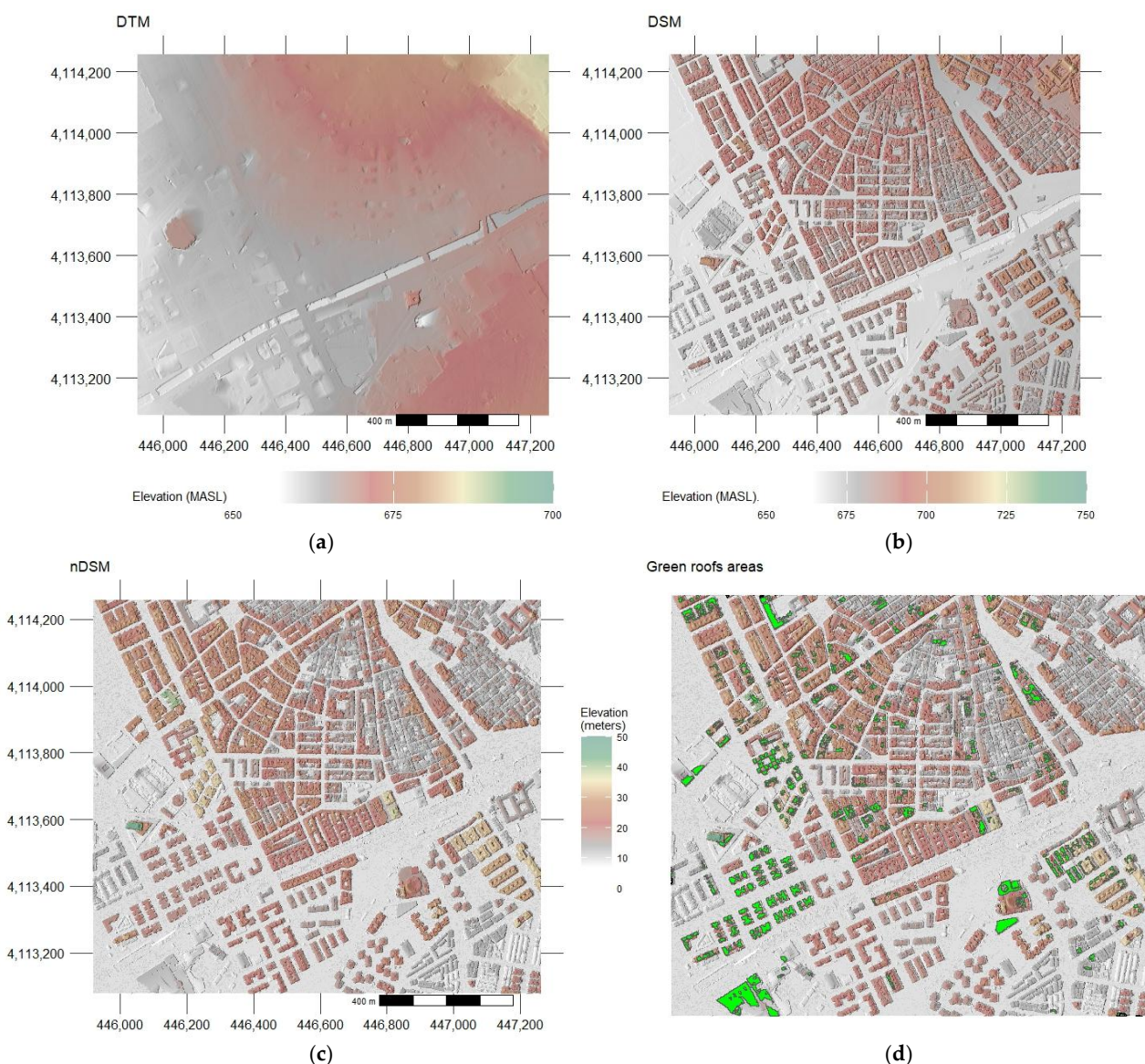


Figure 8. Digital elevation models. (a) Digital Terrain Model, (b) Digital Surface Model, (c) Normalized Digital Surface Model, and (d) selected areas for green roofs shown in green. For visualization purposes, only a portion of the study area is displayed.

2.9. Random Forest

Random Forest (RF) is a machine learning algorithm proposed by Breiman [78]. It is capable of processing very large datasets [79]. It utilizes an ensemble of decision trees to forecast a response variable by learning decision-making rules, making it a smart choice for accurate predictions.

In this study, a RF regression model is implemented in R through the *ranger* package (version 0.16.0) [80] to predict LST by using GRs. Since the LST Landsat image is a 30 m resolution, aggregation was performed in QGIS of all parameters to coincide with the image. LST is the dependent variable, while the NDVI, NDBI, PV, NDWI, WD, SVF, and LCZ are considered the predictors or independent variables. For the RF model, the data is divided into training, validation, and testing sets. Specifically, 60% of the 14 LST images are used for training, 20% for validation, and 20% for testing. This results in 8 LST images allocated for training, 3 images for validation, and 3 images for testing. Additionally, hyperparameter tuning is evaluated based on the lowest root mean square error (*RMSE*) to perform the best

combination of the number of trees (*ntree*) and the number of features randomly selected at each split (*mtry*).

Furthermore, feature importance is computed to assess the influence of each feature based on its predictive power, applying the permutation method [81] that evaluates how much a model's prediction error increases when a specific feature's values are randomly shuffled [82].

In addition to identifying feature importance, we also want to understand the way these features influence model prediction on average—the feature effect. Accumulated local effects, commonly referred to as ALEs, illustrate the marginal impact that one or two features exert on the predicted LST on average. ALE plots are computationally efficient and more robust against correlated features [83].

2.10. Error Metrics

Various error metrics are usually evaluated to determine goodness of fit in regression models of supervised machine learning. In this study, widely used metrics, including the *RMSE*, the mean absolute percentage error (*MAPE*), and the coefficient of determination (*R*²), are employed. *R*² is strongly suggested for model performance evaluation [84]. The metrics are given by

$$R^2 = 1 - \frac{\sum_{i=1}^n (X_i - Y_i)^2}{\sum_{i=1}^n (\bar{Y} - Y_i)^2} \quad (5)$$

$$RMSE = \sqrt{\frac{1}{n} \sum_{i=1}^n (X_i - Y_i)^2} \quad (6)$$

$$MAPE = \frac{100}{n} \sum_{i=1}^n \left| \frac{Y_i - X_i}{Y_i} \right| \quad (7)$$

where X_i is the predicted value, Y_i is the observed value, and n is the total amount of data. The *RMSE* and *MAPE* are performance metrics where the best value = 0 and the worst value = $+\infty$. *R*² values vary from 0 = worst value and 1 = high precision.

2.11. Green Roofs Simulation Approach

We simulate the impact of green roofs after identifying suitable areas for retrofitting, as outlined in Section 2.8. For this purpose, we modified the pixels of the NDVI, NDBI and PV spectral indices at a resolution of 10 m and then resampled to 30 m. Our assumption is that land cover is replaced with vegetation using extensive green roofs, characterized by a substrate depth of <15 cm, resulting in conditions between medium and dense vegetation. Values of the NDVI can range between 0.3 and 0.6 [68]. In addition, through analyses of vegetation values in a park of the city (Figure A1), we determined that an NDVI value of 0.40 and an NDBI value of −0.15 should be assigned. Replacing values from Sentinel-2 was preferred since Landsat 8–9 provides indices at a 30 m resolution cell size, which is bigger than most of the available areas for GRs. Similar approaches were employed by A. Kafy et al. and M. Y. Joshi et al. [85,86].

3. Results and Discussion

3.1. Green Roofs Potential Suitable Areas in Different LCZs

Identifying priority areas is required for effective planning, as discussed in Section 2.11. This decision relates to the availability of each LCZ. By prioritizing these areas, we can more effectively address UHI mitigation and enhance our urban environments.

Mean values of LST on different LCZs are summarized in Table 3. Built-up areas (LCZ-2, 3, 4, 5, 6, and 8) present higher temperatures than natural landscapes (LCZ A and B), demonstrating the impact of trees and green spaces in Granada. Furthermore,

LCZ-6 exhibited lower temperatures than its similar zones, likely due to better ventilation and a greater presence of plant cover [87]. In contrast, LCZ-8 exhibits high LST impact, characterized by large industrial or commercial buildings, along with LCZ-3.

Table 3. Mean LST ($^{\circ}$ C) across different LCZs in Granada.

LCZ2	LCZ3	LCZ4	LCZ5	LCZ6	LCZ8	LCZ9	LCZA	LCZB	LCZC	LCZD	LCZE	LCZF
45.9	47.1	45.8	46.1	44.9	49.8	43.4	41.5	42.8	46.3	45.7	48.7	49.4

Figure 9a illustrates the total area available for each LCZ in Granada. Notably, LCZ-2 and LCZ-5 have the largest available areas, accounting for 40% and 45% of the total 38 hectares suitable, respectively. Each of these zones exceed 150,000 m^2 (Figure 9b). In contrast, LCZ-3, LCZ-4, LCZ-6, and LCZ-8 represent only 2% to 4% of the total area. Unfortunately, LCZ-3 and LCZ-8 have little GRs area available.

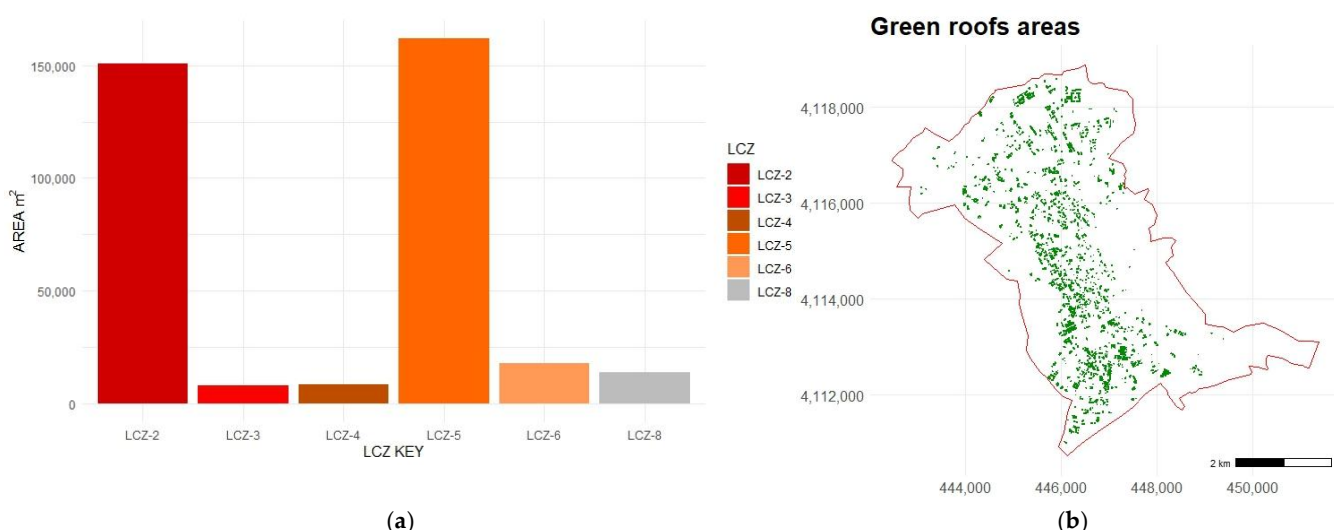


Figure 9. (a) The total available area (in m^2) within each Local Climate Zone in Granada, and (b) overall distribution of green roof-suitable areas across the city.

3.2. Random Forest Regression Model Results

RF was performed with the obtained pixels from the 30 m grid, which were split into training data = 8 images, validation data = 3 images, and testing data = 3 images. Hyperparameter optimization was based on the lowest RMSE, resulting in mtry = 4 and ntree = 800 (Table A1).

The model exhibited very good results: $R^2 = 0.95$ for training with an RMSE = 0.79 $^{\circ}$ C; meanwhile, $R^2 = 0.69$ for validation and RMSE = 1.83 $^{\circ}$ C.

Following model training, performance was evaluated using the testing data, which included three unseen images reserved for this stage. Model performance for test data exhibited an $R^2 = 0.68$ and an RMSE value of 1.59 $^{\circ}$ C. Additionally, MAPE values remained below 4%. Figure 10 shows the scatter plot for the model, with an ideal tendency in red. The RMSE value is acceptable, given that its standard deviation, SD = 2.31, falls within the range of SD = 1.12 RMSE–2.2 RMSE [88]. Metric errors are presented in Table 4.

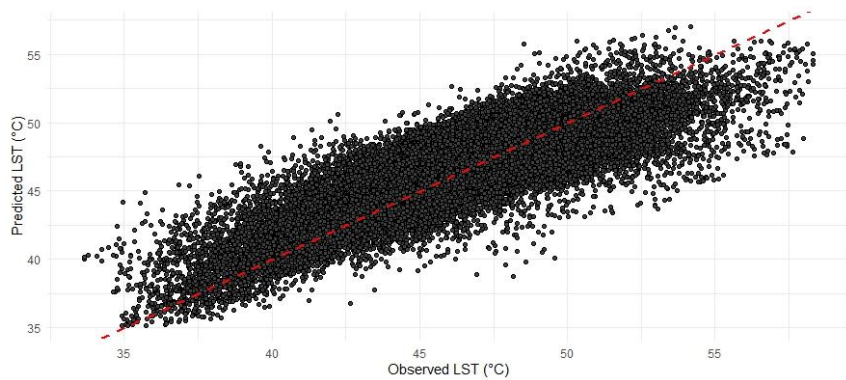


Figure 10. Scatterplot of observations vs. predictions for the testing set, which consists of three LST images. The red dashed line is the ideal prediction.

Table 4. General error metrics for the training, validation, and testing stages of the Random Forest model.

	RMSE (°C)	MAPE (%)	R ²
Training	0.791	1.371	0.95
Validation	1.836	3.319	0.69
Testing	1.599	2.639	0.68

These results show that the model consistently performed well using all the features, confirming its reliability in predicting new surface temperatures. The feature importance of parameters is depicted in Figure 11. The NDVI feature has the highest importance, indicating vegetation strongly influences LST. WD and the SVF are also significant contributors, while PV has a lower impact. Notably, the NDBI appears to perform weakly compared to the NDVI in this scenario; one possible explanation might be that the NDVI is negatively correlated with the NDBI [89]. However, we can evaluate this further with an interaction ALE plot of two features.

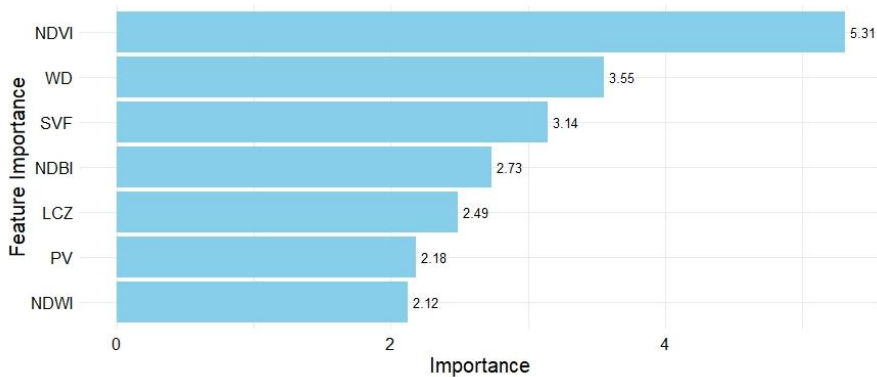


Figure 11. The permutation feature importance for each parameter in predicting LST.

ALE plots enhance model interpretation and reveal nonlinear relationships among features. In Granada, the differences in the NDVI (Figure 12a) reveal valuable nonlinear variations in LST. At low values of NDVI (below 0), the LST starts to decrease a little, perhaps because bare soil or mixed land cover types between urban and vegetation affect temperature differently. Beyond 0–0.5, the NDVI shows an important decrease in temperature, reaching a stable point at 0.5, with an average decrease of 4 °C.

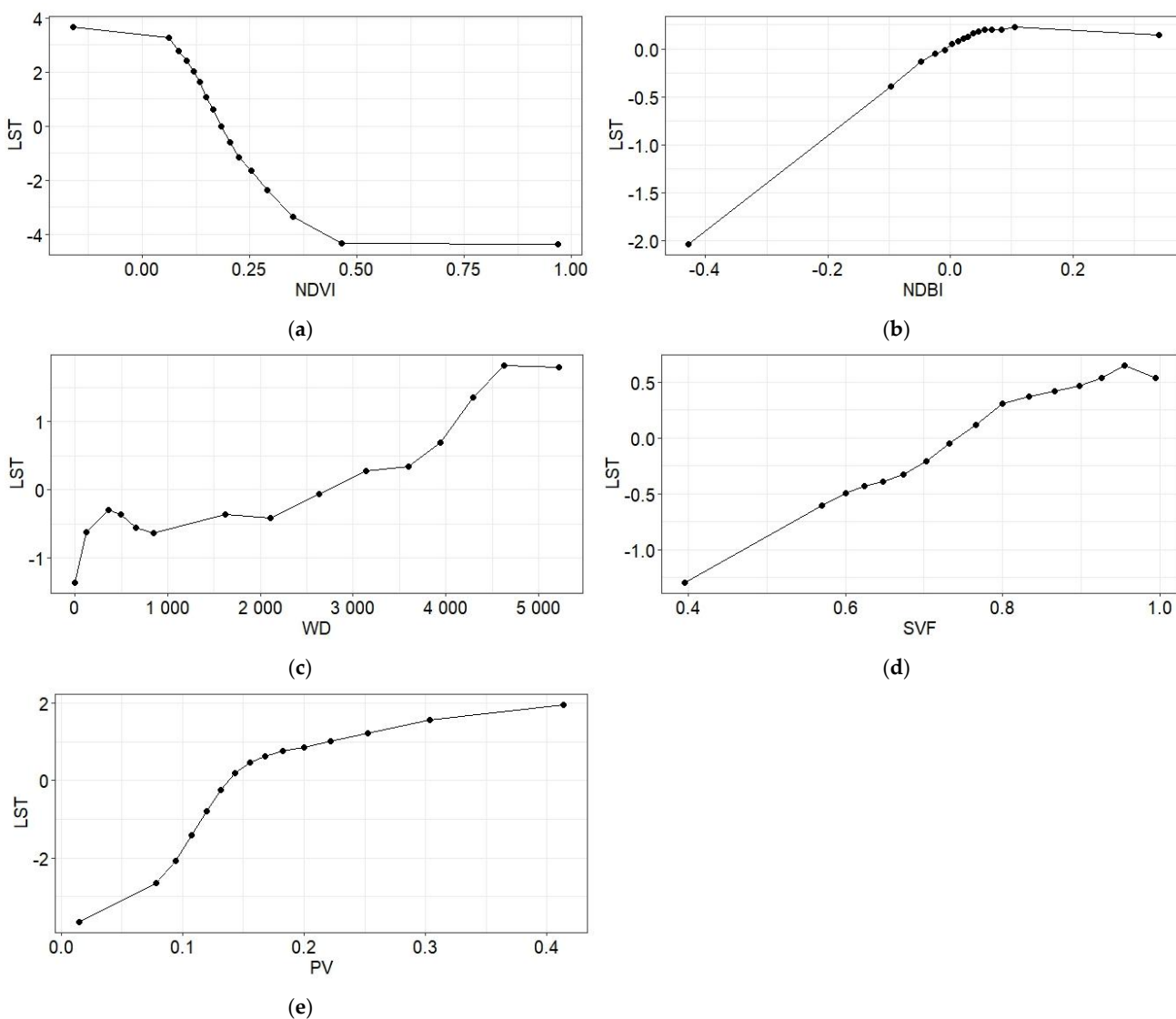


Figure 12. ALE plots for five influencing factors: (a) NDVI, (b) NDBI, (c) distance to water bodies, (d) SVF, and (e) PV. LST is influenced nonlinearly by most factors, except the SVF, which has an almost linear effect.

On the other hand, stronger variations are observed with changes in the NDBI, showing nonlinear positive correlation with LST (Figure 12b). This is in agreement with studies analyzing the behavior of key variables in relation to LST [58,89,90]. From values of -0.40 to 0 , the NDBI increased by $2\text{ }^{\circ}\text{C}$ and remained steady after 0 . Distance to water bodies presents a positive correlation with LST (Figure 12c), confirming its important benefit in cities [91]. The SVF shows a positive almost linear association with LST and decreases around $1\text{ }^{\circ}\text{C}$ in close areas (Figure 12d). Other features like PV and the NDWI show little interaction with LST and were omitted.

LST was influenced nonlinearly by most factors, including the NDVI, NDBI, WD, and PV; however, the influence of the SVF on LST is almost linear.

We need to analyze the relationship between both indexes and determine whether vegetation is a key factor. To achieve this, we explore their effect on LST using an ALE plot of two features at once. Figure 13 illustrates those lower values of the NDBI, which are associated with vegetation and water bodies, along with different values of the NDVI, correlated with lower LST. This suggests that vegetation plays a significant role in temperature

regulation in Granada during summer months. Consequently, the model has learned that vegetation presence contributes to decreasing LST.

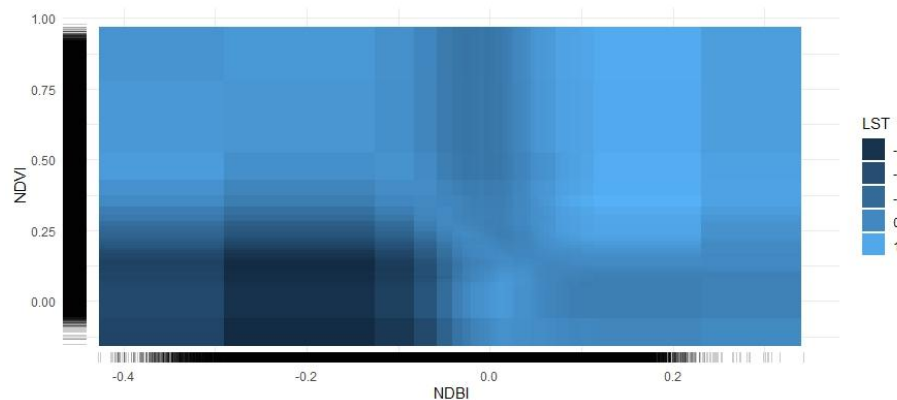


Figure 13. ALE plot for LST and the interaction between the NDVI and NDBI.

3.3. Results on Temperature Mitigation Using Green Roofs

The results of the LST mitigation strategy using extensive GRs for suitable buildings are depicted in Figure 14. For this purpose, testing data was employed to model LST values with GRs by modifying the NDVI, NDBI, and PV, as explained in Section 2.11. The pixels containing and surrounding the potential rooftop areas, a total of 2800 pixels, were compared against predicted LST values. The model demonstrates a reduction in temperature across most pixels. An average decrease of 1.45 °C is obtained.

After obtaining the results of the model with the modified pixels (incorporating GRs), a small number of pixels (207) showed a slight increase in temperature. Since having an increment of temperature when vegetation is incorporated is unrealistic [92–94], these pixels were converted to zero.

3.4. Comparative Analysis and Discussion

Some studies have used machine learning algorithms to predict GR implementation. A. Asadi et al. [74] used an artificial neural network (ANN) for a case study in Austin, Texas. They reported an average decrease of 1.96 °C. In the same city, A. Kafy et al. [85] followed a similar approach, obtaining an average LST decrease of 2.80 °F (1.55 °C) by using higher resolution data. In two Belgian cities, M. Y. Joshi et al. [86] employed a RF model, obtaining an average LST reduction of 0.67 °C by implementing intensive GRs. The results of the previous studies show a moderate reduction in LST, which is similar to the result obtained in the present research.

Numerous studies have used machine learning algorithms to explore the effects of LST in cities [58,95,96]. For instance, D. Han et al. [95] used RF and boosted regression trees to understand the nonlinear effects of 2D/3D urban landscapes on diurnal LST, concluding that vegetation and building metrics are domain factors affecting LST during daytime. This is in accordance with our results that emphasizes the importance of NDBI in LST.

In addition, some studies have employed different approaches to assess the impact of green roofs; for example, ENVI-met, commonly used for urban climatology and building design purposes, helps explore the effects of green infrastructure at the microscale level [52,97,98]. In this model, Susca et al. [99] modeled different scenarios and found that in Rome, which is also categorized as having a Csa climate, the use of GRs alone as a UHI mitigation strategy is negligible. This finding aligns with our results using RF, which also indicates a moderate impact in Granada with a Csa climate.

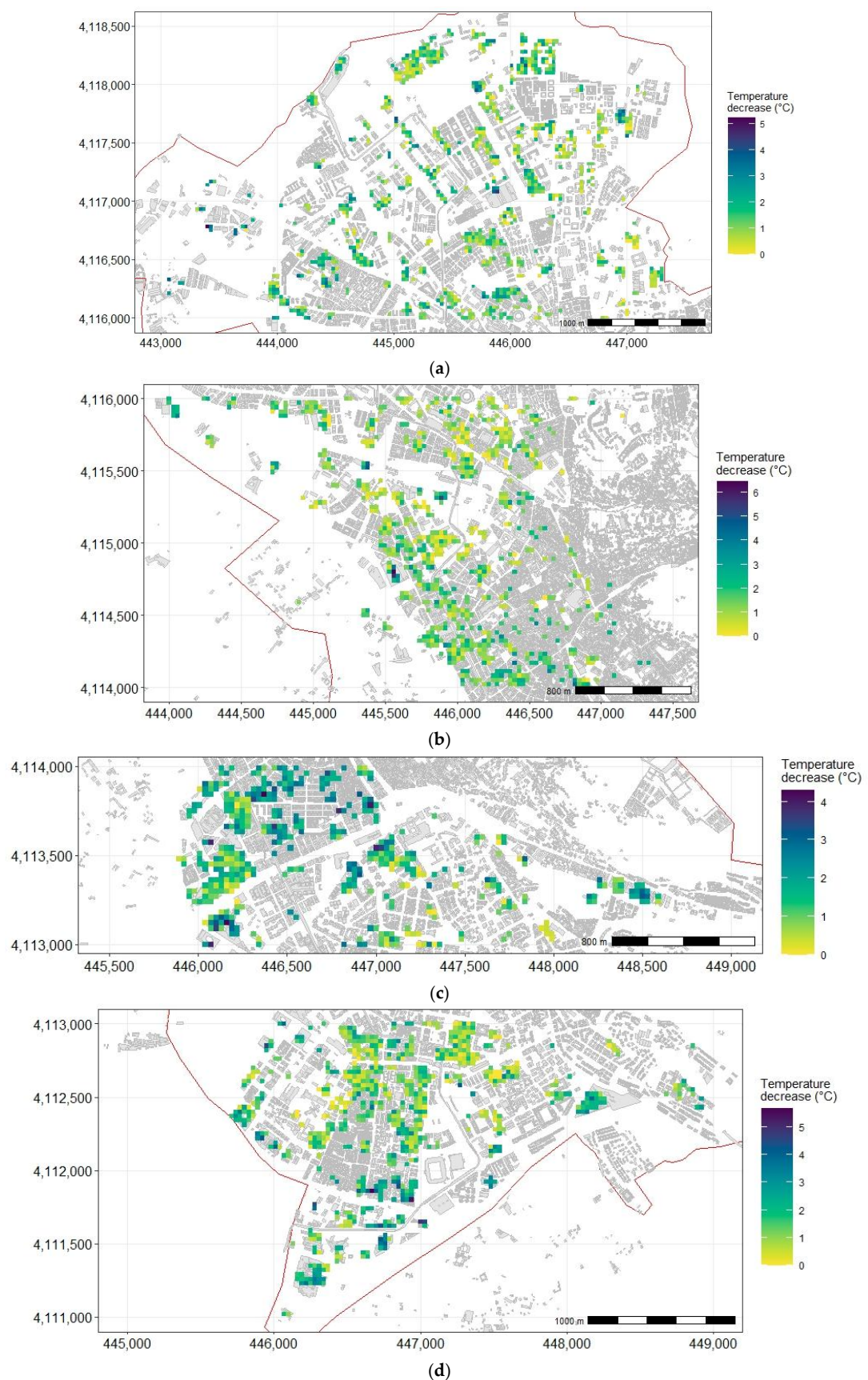


Figure 14. Temperature reduction achieved by green roofs. (a) Northern area of Granada. (b) City center. (c) Downtown City center. (d) Southern area.

3.5. Limitations and Recommendations

In the present study, it has been assumed that GRs could be installed on all selected buildings; however, they must be separated and detailed for public and private buildings. General interest has been raised due to the advantages of installing GRs, especially in public buildings rather than private ones, due to high installation and maintenance costs [100,101]. Hence, increasing the area available for GRs might be even harder to accomplish.

In a Mediterranean context, the problem relies on future climate projections. Tuel and Eltahir [2] discussed Climate Change's impact on Mediterranean precipitation patterns using various climatology datasets, suggesting a potential decline in rainfall. With the increased frequency of drought seasons, there may be a greater risk of water scarcity [102]; it can be challenging to maintain dense vegetation coverage on GRs, which is an important factor in reducing air and land surface temperatures. This was attested to with thermal photography in a real GR, as described in Section 2.7. Granada requires urgent interventions to combat elevated temperatures affecting building energy use and incrementing energy demand [103]—for instance, changing materials to increase albedo, thereby reducing temperature absorption, and urban planning at street level, such as planting trees to increase shade [104–106].

4. Conclusions

In this research, we assess the impact of retrofitting green roofs (GRs) in a semi-arid climate, aiming to reduce land surface temperature (LST) during daytime. A Random Forest (RF) model was used to predict the LST impact, and remote sensing metrics were included to obtain the inputs of the model. The analysis of feature importance indicated that the NDVI, WD, SVF, and NDBI control predictions.

The results of this study provide more precise directions for future investigations employing the Random Forest machine learning technique to capture the dynamics of LST at city scale and to examine the importance of different urban features and their nonlinear effects on LST. The originality of our research lies in building a robust and reliable model for predicting LST, which was trained, validated, and tested using a large dataset.

This research evaluates the effect of GRs in a city with semi-arid climate in southern Spain in the Mediterranean area. Furthermore, this model was not limited to specific urban zones; instead, it was developed at an entire city scale where no studies have yet been conducted, paving the way for a new understanding of LST dynamics and identifying critical areas in any city using open-source data. Additional findings were as follows:

- The proposed model predicts an average LST reduction of 1.45 °C during the hot months in summer, indicating that the potential of extensive green roofs in the city to mitigate high LST is moderate.
- The selection process to identify areas suitable for retrofitting GRs with the help of LiDAR points identified fewer suitable areas for green roofs than the total number of existing roofs available. Three criteria were considered for selecting these areas: slopes lower than 15% to enhance stormwater retention, lower slopes to prevent erosion issues, and the exclusion of small areas that might not have significant influence, leading to a more realistic assessment of potential retrofitting opportunities. Thus, the effects of GRs alone might be neglectable to mitigate high LST.
- The results indicate different LSTs between built-up areas and landscape zones. However, the difference in temperature between urban built-up areas is small, suggesting that all urban LCZs are equally a priority for greening.
- In Granada, LCZ-2 and 5 present more available areas suitable for retrofitting GRs, while LCZ 8, with a high land surface temperature, does not have enough space

for green roofs, requiring urgent intervention with different planning to lower the temperature.

- Permutation feature importance highlights the crucial role of the NDVI in interacting with LST. And the ALE plot shows the marginal correlation of the NDVI and LST to be important.
- The model is able to predict not only extensive green roofs, but it could also be modified for using intensive green roofs, characterized by higher and denser vegetation and therefore higher NDVI values. Additionally, the model can simulate the placing of larger green spaces such as parks and predict LST reduction.

Addressing the UHI effect in semi-arid cities is crucial, as it is worsening annually and poses significant health risks to residents. This study suggests that multiple measures apart from greening are necessary to combat UHI effects. The findings of this study can assist urban planners developing more effective strategies to mitigate the UHI effect and enhance thermal comfort in urban areas. Hopefully, this paper fills the gap of understanding the role of introducing GRs as greening solutions that can mitigate the temperature in semi-arid cities.

Author Contributions: Conceptualization, F.S.-C., L.N., D.H.-G. and S.R.L.-C.; methodology, F.S.-C., L.N. and D.H.-G.; validation, F.S.-C.; formal analysis, F.S.-C., D.H.-G. and S.R.L.-C.; investigation, F.S.-C. and D.H.-G.; data curation, F.S.-C.; writing—original draft preparation, F.S.-C.; writing—review and editing, F.S.-C., L.N., D.H.-G. and S.R.L.-C.; visualization, F.S.-C.; project administration, L.N.; funding acquisition, L.N. All authors have read and agreed to the published version of the manuscript.

Funding: This work has been supported by the European Union's FEDER program, IFMIF-DONES Junta de Andalucía's program at the Universidad de Granada, Spain (SE21_UGR_IFMIF-DONES FEDER).

Data Availability Statement: The data regarding this research is available on request to the authors.

Conflicts of Interest: The authors declare no conflicts of interest.

Appendix A

Evaluating possible NDVI and NDBI values to replace and simulate green roofs.



Figure A1. Zonal statistics of the NDVI and NDBI in a park in Granada are analyzed, and potential values from this park are also considered for modifying the NDVI and NDBI in order to estimate green roofs.

Hyperparameter mtry and ntree selection is shown in Table A1.

Table A1. Random Forest hyperparameter tuning for mtry and ntree. The combination with the lowest RMSE is highlighted in yellow.

mtry	ntree	RMSE
3	400	1.841685
3	500	1.841322
3	400	1.841685
3	500	1.841322
3	600	1.841658
3	700	1.841122
3	800	1.840762
4	400	1.837626
4	500	1.837586
4	600	1.837157
4	700	1.837165
4	800	1.836764
5	400	1.841444
5	500	1.840638
5	600	1.840351
5	700	1.839835
5	800	1.839432
6	400	1.847772
6	500	1.846869
6	600	1.846509
6	700	1.845937
6	800	1.846129
7	400	1.856779
7	500	1.857391
7	600	1.857304
7	700	1.856979
7	800	1.856862

References

- Rama, H.O.; Roberts, D.; Tignor, M.; Poloczanska, E.S.; Mintenbeck, K.; Alegría, A.; Craig, M.; Langsdorf, S.; Löschke, S.; Möller, V.; et al. *Climate Change 2022: Impacts, Adaptation and Vulnerability Working Group II Contribution to the Sixth Assessment Report of the Intergovernmental Panel on Climate Change*; IPCC: Geneva, Switzerland, 2022.
- Tuel, A.; Eltahir, E.A.B. Why Is the Mediterranean a Climate Change Hot Spot? *J. Clim.* **2020**, *33*, 5829–5843. [[CrossRef](#)]
- Ribas, A.; Olcina, J.; Sauri, D. More exposed but also more vulnerable? Climate change, high intensity precipitation events and flooding in Mediterranean Spain. *Disaster Prev. Manag. Int. J.* **2020**, *29*, 229–248. [[CrossRef](#)]
- Mora, C.; Dousset, B.; Caldwell, I.R.; Powell, F.E.; Geronimo, R.C.; Bielecki, C.R.; Counsell, C.W.W.; Dietrich, B.S.; Johnston, E.T.; Louis, L.V.; et al. Global risk of deadly heat. *Nat. Clim. Change* **2017**, *7*, 501–506. [[CrossRef](#)]
- Aflaki, A.; Mirnezhad, M.; Ghaffarianhoseini, A.; Ghaffarianhoseini, A.; Omrany, H.; Wang, Z.-H.; Akbari, H. Urban heat island mitigation strategies: A state-of-the-art review on Kuala Lumpur, Singapore and Hong Kong. *Cities* **2017**, *62*, 131–145. [[CrossRef](#)]

6. Zhao, Y.; Sen, S.; Susca, T.; Iaria, J.; Kibilay, A.; Gunawardena, K.; Zhou, X.; Takane, Y.; Park, Y.; Wang, X.; et al. Beating urban heat: Multimeasure-centric solution sets and a complementary framework for decision-making. *Renew. Sustain. Energy Rev.* **2023**, *186*, 113668. [[CrossRef](#)]
7. Hidalgo García, D.; Arco Díaz, J.; Martín Martín, A.; Gómez Cobos, E. Spatiotemporal Analysis of Urban Thermal Effects Caused by Heat Waves through Remote Sensing. *Sustainability* **2022**, *14*, 12262. [[CrossRef](#)]
8. Degirmenci, K.; Desouza, K.C.; Fieuw, W.; Watson, R.T.; Yigitcanlar, T. Understanding policy and technology responses in mitigating urban heat islands: A literature review and directions for future research. *Sustain. Cities Soc.* **2021**, *70*, 102873. [[CrossRef](#)]
9. Susca, T.; Pomponi, F. Heat island effects in urban life cycle assessment: Novel insights to include the effects of the urban heat island and UHI-mitigation measures in LCA for effective policy making. *J. Ind. Ecol.* **2020**, *24*, 410–423. [[CrossRef](#)]
10. Yang, J.; Hu, L.; Wang, C. Population dynamics modify urban residents' exposure to extreme temperatures across the United States. *Sci. Adv.* **2019**, *5*, eaay3452. [[CrossRef](#)]
11. Pena Acosta, M.; Vahdatikhaki, F.; Santos, J.; Hammad, A.; Dorée, A.G. How to bring UHI to the urban planning table? A data-driven modeling approach. *Sustain. Cities Soc.* **2021**, *71*, 102948. [[CrossRef](#)]
12. Fleck, R.; Gill, R.L.; Saadeh, S.; Pettit, T.; Wooster, E.; Torpy, F.; Irga, P. Urban green roofs to manage rooftop microclimates: A case study from Sydney, Australia. *Build. Environ.* **2022**, *209*, 108673. [[CrossRef](#)]
13. Xiang, Y.; Yuan, C.; Cen, Q.; Huang, C.; Wu, C.; Teng, M.; Zhou, Z. Heat risk assessment and response to green infrastructure based on local climate zones. *Build. Environ.* **2024**, *248*, 111040. [[CrossRef](#)]
14. Lemus-Canovas, M.; Martin-Vide, J.; Moreno-Garcia, M.C.; Lopez-Bustins, J.A. Estimating Barcelona's metropolitan daytime hot and cold poles using Landsat-8 Land Surface Temperature. *Sci. Total Environ.* **2020**, *699*, 134307. [[CrossRef](#)] [[PubMed](#)]
15. Ward, K.; Lauf, S.; Kleinschmit, B.; Endlicher, W. Heat waves and urban heat islands in Europe: A review of relevant drivers. *Sci. Total Environ.* **2016**, *569–570*, 527–539. [[CrossRef](#)]
16. He, B.-J.; Wang, J.; Liu, H.; Ulpiani, G. Localized synergies between heat waves and urban heat islands: Implications on human thermal comfort and urban heat management. *Environ. Res.* **2021**, *193*, 110584. [[CrossRef](#)]
17. Campbell, S.; Remenyi, T.A.; White, C.J.; Johnston, F.H. Heatwave and health impact research: A global review. *Health Place* **2018**, *53*, 210–218. [[CrossRef](#)] [[PubMed](#)]
18. An, N.; Dou, J.; González-Cruz, J.E.; Bornstein, R.D.; Miao, S.; Li, L. An Observational Case Study of Synergies between an Intense Heat Wave and the Urban Heat Island in Beijing. *J. Appl. Meteorol. Climatol.* **2020**, *59*, 605–620. [[CrossRef](#)]
19. Hidalgo-García, D.; Arco-Díaz, J. Modeling the Surface Urban Heat Island (SUHI) to study of its relationship with variations in the thermal field and with the indices of land use in the metropolitan area of Granada (Spain). *Sustain. Cities Soc.* **2022**, *87*, 104166. [[CrossRef](#)]
20. Song, J.; Chen, W.; Zhang, J.; Huang, K.; Hou, B.; Prishchepov, A.V. Effects of building density on land surface temperature in China: Spatial patterns and determinants. *Landsc. Urban Plan.* **2020**, *198*, 103794. [[CrossRef](#)]
21. Zhang, R.; Corte-Real, J.; Moreira, M.; Kilsby, C.; Burton, A.; Fowler, H.J.; Blenkinsop, S.; Birkinshaw, S.; Forsythe, N.; Nunes, J.P. Downscaling climate change of mean climatology and extremes of precipitation and temperature: Application to a Mediterranean climate basin. *Int. J. Climatol.* **2019**, *39*, 4985–5005. [[CrossRef](#)]
22. Serrano-Notivoli, R.; Lemus-Canovas, M.; Barrao, S.; Sarricolea, P.; Meseguer-Ruiz, O.; Tejedor, E. Heat and cold waves in mainland Spain: Origins, characteristics, and trends. *Weather Clim. Extrem.* **2022**, *37*, 100471. [[CrossRef](#)]
23. Santamouris, M. Recent progress on urban overheating and heat island research. Integrated assessment of the energy, environmental, vulnerability and health impact. Synergies with the global climate change. *Energy Build.* **2020**, *207*, 109482. [[CrossRef](#)]
24. Amani-Beni, M.; Chen, Y.; Vasileva, M.; Zhang, B.; Xie, G.-D. Quantitative-spatial relationships between air and surface temperature, a proxy for microclimate studies in fine-scale intra-urban areas? *Sustain. Cities Soc.* **2022**, *77*, 103584. [[CrossRef](#)]
25. Berardi, U.; Jandaghian, Z.; Graham, J. Effects of greenery enhancements for the resilience to heat waves: A comparison of analysis performed through mesoscale (WRF) and microscale (Envi-met) modeling. *Sci. Total Environ.* **2020**, *747*, 141300. [[CrossRef](#)]
26. Kappou, S.; Souliotis, M.; Papaefthimiou, S.; Panaras, G.; Paravantis, J.A.; Michalena, E.; Hills, J.M.; Vouros, A.P.; Ntymenou, A.; Mihalakakou, G. Cool Pavements: State of the Art and New Technologies. *Sustainability* **2022**, *14*, 5159. [[CrossRef](#)]
27. Mourou, C.; Zamorano, M.; Ruiz, D.P.; Martín-Morales, M. Cool Surface Strategies with an Emphasis on the Materials Dimension: A Review. *Appl. Sci.* **2022**, *12*, 1893. [[CrossRef](#)]
28. He, Q.; Tapia, F.; Reith, A. Quantifying the influence of nature-based solutions on building cooling and heating energy demand: A climate specific review. *Renew. Sustain. Energy Rev.* **2023**, *186*, 113660. [[CrossRef](#)]
29. Susca, T. Nature-based solutions applied to the built environment to alleviate climate change: Benefits, co-benefits, and trade-offs in a geographical multi-scale perspective. In *Handbook of Climate Change Mitigation and Adaptation*; Springer: Berlin/Heidelberg, Germany, 2022; pp. 2117–2167.

30. Leite, F.R.; Antunes, M.L.P. Green roof recent designs to runoff control: A review of building materials and plant species used in studies. *Ecol. Eng.* **2023**, *189*, 106924. [[CrossRef](#)]
31. Cascone, S. Green roof design: State of the art on technology and materials. *Sustainability* **2019**, *11*, 3020. [[CrossRef](#)]
32. Susca, T.; Zanghirella, F.; Colasuonno, L.; Del Fatto, V. Effect of green wall installation on urban heat island and building energy use: A climate-informed systematic literature review. *Renew. Sustain. Energy Rev.* **2022**, *159*, 112100. [[CrossRef](#)]
33. Bevilacqua, P. The effectiveness of green roofs in reducing building energy consumptions across different climates. *A Summ. Lit. Results Renew. Sustain. Energy Rev.* **2021**, *151*, 111523. [[CrossRef](#)]
34. Solecki, W.D.; Rosenzweig, C.; Parshall, L.; Pope, G.; Clark, M.; Cox, J.; Wiencke, M. Mitigation of the heat island effect in urban New Jersey. *Glob. Environ. Change Part B Environ. Hazards* **2005**, *6*, 39–49. [[CrossRef](#)]
35. Sharma, A.; Conry, P.; Fernando, H.; Hamlet, A.F.; Hellmann, J.; Chen, F. Green and cool roofs to mitigate urban heat island effects in the Chicago metropolitan area: Evaluation with a regional climate model. *Environ. Res. Lett.* **2016**, *11*, 064004. [[CrossRef](#)]
36. Wong, N.H.; Tan, C.L.; Kolokotsa, D.D.; Takebayashi, H. Greenery as a mitigation and adaptation strategy to urban heat. *Nat. Rev. Earth Environ.* **2021**, *2*, 166–181. [[CrossRef](#)]
37. Decina, S.M.; Templer, P.H.; Hutyra, L.R. Atmospheric inputs of nitrogen, carbon, and phosphorus across an urban area: Unaccounted fluxes and canopy influences. *Earth's Future* **2018**, *6*, 134–148. [[CrossRef](#)]
38. Kavehei, E.; Jenkins, G.A.; Adame, M.F.; Lemckert, C. Carbon sequestration potential for mitigating the carbon footprint of green stormwater infrastructure. *Renew. Sustain. Energy Rev.* **2018**, *94*, 1179–1191. [[CrossRef](#)]
39. Ondoño, S.; Martínez-Sánchez, J.J.; Moreno, J.L. Chapter 7—Carbon and Nitrogen Sequestration Potential of Mediterranean Green Roofs Prototypes. In *Soil Management and Climate Change*; Muñoz, M.Á., Zornoza, R., Eds.; Academic Press: Cambridge, MA, USA, 2018; pp. 85–102.
40. Prigioniero, A.; Zuzolo, D.; Niinemets, Ü.; Guarino, C. Nature-based solutions as tools for air phytoremediation: A review of the current knowledge and gaps. *Environ. Pollut.* **2021**, *277*, 116817. [[CrossRef](#)]
41. Shafique, M.; Xue, X.; Luo, X. An overview of carbon sequestration of green roofs in urban areas. *Urban For. Urban Green.* **2020**, *47*, 126515. [[CrossRef](#)]
42. Arbid, Y.; Richard, C.; Sleiman, M. Towards an experimental approach for measuring the removal of urban air pollutants by green roofs. *Build. Environ.* **2021**, *205*, 108286. [[CrossRef](#)]
43. Hewitt, C.N.; Ashworth, K.; MacKenzie, A.R. Using green infrastructure to improve urban air quality (GI4AQ). *Ambio* **2020**, *49*, 62–73. [[CrossRef](#)]
44. Di Sabatino, S.; Barbano, F.; Brattich, E.; Pulvirenti, B. The Multiple-Scale Nature of Urban Heat Island and Its Footprint on Air Quality in Real Urban Environment. *Atmosphere* **2020**, *11*, 1186. [[CrossRef](#)]
45. Porcaro, M.; Ruiz de Adana, M.; Comino, F.; Peña, A.; Martín-Consuerga, E.; Vanwalleghem, T. Long term experimental analysis of thermal performance of extensive green roofs with different substrates in Mediterranean climate. *Energy Build.* **2019**, *197*, 18–33. [[CrossRef](#)]
46. Vilar, M.L.; Tello, L.; Hidalgo, A.; Bedoya, C. An energy balance model of heterogeneous extensive green roofs. *Energy Build.* **2021**, *250*, 111265. [[CrossRef](#)]
47. He, Y.; Yu, H.; Dong, N.; Ye, H. Thermal and energy performance assessment of extensive green roof in summer: A case study of a lightweight building in Shanghai. *Energy Build.* **2016**, *127*, 762–773. [[CrossRef](#)]
48. Detommaso, M.; Costanzo, V.; Nocera, F.; Evola, G. Evaluation of the cooling potential of a vertical greenery system coupled to a building through an experimentally validated transient model. *Build. Environ.* **2023**, *244*, 110769. [[CrossRef](#)]
49. Wooster, E.I.F.; Fleck, R.; Torpy, F.; Ramp, D.; Irga, P.J. Urban green roofs promote metropolitan biodiversity: A comparative case study. *Build. Environ.* **2022**, *207*, 108458. [[CrossRef](#)]
50. Li, M.; Remme, R.P.; van Bodegom, P.M.; van Oudenhoven, A.P.E. Solution to what? Global assessment of nature-based solutions, urban challenges, and outcomes. *Landscape Urban Plan.* **2025**, *256*, 105294. [[CrossRef](#)]
51. Jato-Espino, D.; Manchado, C.; Roldán-Valcarce, A.; Moscardó, V. ArcUHI: A GIS add-in for automated modelling of the Urban Heat Island effect through machine learning. *Urban Clim.* **2022**, *44*, 101203. [[CrossRef](#)]
52. Balany, F.; Ng, A.W.; Muttill, N.; Muthukumaran, S.; Wong, M.S. Green Infrastructure as an Urban Heat Island Mitigation Strategy—A Review. *Water* **2020**, *12*, 3577. [[CrossRef](#)]
53. Nastran, M.; Kobal, M.; Eler, K. Urban heat islands in relation to green land use in European cities. *Urban For. Urban Green.* **2019**, *37*, 33–41. [[CrossRef](#)]
54. Marando, F.; Heris, M.P.; Zulian, G.; Udías, A.; Mentaschi, L.; Chrysoulakis, N.; Parastatidis, D.; Maes, J. Urban heat island mitigation by green infrastructure in European Functional Urban Areas. *Sustain. Cities Soc.* **2022**, *77*, 103564. [[CrossRef](#)]
55. Chen, D.; Zhang, F.; Zhang, M.; Meng, Q.; Jim, C.Y.; Shi, J.; Tan, M.L.; Ma, X. Landscape and vegetation traits of urban green space can predict local surface temperature. *Sci. Total Environ.* **2022**, *825*, 154006. [[CrossRef](#)] [[PubMed](#)]
56. Gao, Y.; Zhao, J.; Han, L. Quantifying the nonlinear relationship between block morphology and the surrounding thermal environment using random forest method. *Sustain. Cities Soc.* **2023**, *91*, 104443. [[CrossRef](#)]

57. Wang, Q.; Wang, X.; Meng, Y.; Zhou, Y.; Wang, H. Exploring the impact of urban features on the spatial variation of land surface temperature within the diurnal cycle. *Sustain. Cities Soc.* **2023**, *91*, 104432. [[CrossRef](#)]
58. Li, J. Evaluating the Correlation Between Impacting Factors and Land Surface Temperature via Spatial Regression Model and Random Forest. *Prof. Geogr.* **2024**, *76*, 740–755. [[CrossRef](#)]
59. Kottke, M.; Grieser, J.; Beck, C.; Rudolf, B.; Rubel, F. World map of the Köppen-Geiger climate classification updated. *Meteorol. Z.* **2006**, *15*, 259–263. [[CrossRef](#)]
60. Huang, F.; Jiang, S.; Zhan, W.; Bechtel, B.; Liu, Z.; Demuzere, M.; Huang, Y.; Xu, Y.; Ma, L.; Xia, W.; et al. Mapping local climate zones for cities: A large review. *Remote Sens. Environ.* **2023**, *292*, 113573. [[CrossRef](#)]
61. Stewart, I.D.; Oke, T.R. Local climate zones for urban temperature studies. *Bull. Am. Meteorol. Soc.* **2012**, *93*, 1879–1900. [[CrossRef](#)]
62. Zhou, L.; Yuan, B.; Hu, F.; Wei, C.; Dang, X.; Sun, D. Understanding the effects of 2D/3D urban morphology on land surface temperature based on local climate zones. *Build. Environ.* **2022**, *208*, 108578. [[CrossRef](#)]
63. Anjos, M.; Targino, A.C.; Krecl, P.; Oukawa, G.Y.; Braga, R.F. Analysis of the urban heat island under different synoptic patterns using local climate zones. *Build. Environ.* **2020**, *185*, 107268. [[CrossRef](#)]
64. Demuzere, M.; Kittner, J.; Bechtel, B. LCZ Generator: A web application to create Local Climate Zone maps. *Front. Environ. Sci.* **2021**, *9*, 637455. [[CrossRef](#)]
65. Landsat Mission Management Officer. *Landsat 8-9 Operational Land Imager (OLI)-Thermal Infrared Sensor (TIRS) Collection 2 Level 2 (L2) Data Format Control Book (DFCB)*; United States Geological Survey: Reston, VA, USA, 2020; 78p.
66. Yu, X.; Guo, X.; Wu, Z. Land Surface Temperature Retrieval from Landsat 8 TIRS—Comparison between Radiative Transfer Equation-Based Method, Split Window Algorithm and Single Channel Method. *Remote Sens.* **2014**, *6*, 9829–9852. [[CrossRef](#)]
67. Zha, Y.; Gao, J.; Ni, S. Use of normalized difference built-up index in automatically mapping urban areas from TM imagery. *Int. J. Remote Sens.* **2003**, *24*, 583–594. [[CrossRef](#)]
68. McFeeters, S.K. The use of the Normalized Difference Water Index (NDWI) in the delineation of open water features. *Int. J. Remote Sens.* **1996**, *17*, 1425–1432. [[CrossRef](#)]
69. Lindberg, F.; Grimmond, C.S.B.; Gabey, A.; Huang, B.; Kent, C.W.; Sun, T.; Theeuwes, N.E.; Järvi, L.; Ward, H.C.; Capel-Timms, I. Urban Multi-scale Environmental Predictor (UMEP): An integrated tool for city-based climate services. *Environ. Model. Softw.* **2018**, *99*, 70–87. [[CrossRef](#)]
70. Tabares-Velasco, P.C.; Srebric, J. A heat transfer model for assessment of plant based roofing systems in summer conditions. *Build. Environ.* **2012**, *49*, 310–323. [[CrossRef](#)]
71. Zhao, M.; Tabares-Velasco, P.C.; Srebric, J.; Komarneni, S.; Berghage, R. Effects of plant and substrate selection on thermal performance of green roofs during the summer. *Build. Environ.* **2014**, *78*, 199–211. [[CrossRef](#)]
72. Braun, A.; Warth, G.; Bachofner, F.; Schultz, M.; Hochschild, V. Mapping Urban Structure Types Based on Remote Sensing Data—A Universal and Adaptable Framework for Spatial Analyses of Cities. *Land* **2023**, *12*, 1885. [[CrossRef](#)]
73. Roussel, J.-R.; Auty, D.; Coops, N.C.; Tompalski, P.; Goodbody, T.R.; Meador, A.S.; Bourdon, J.-F.; De Boissieu, F.; Achim, A. lidR: An R package for analysis of Airborne Laser Scanning (ALS) data. *Remote Sens. Environ.* **2020**, *251*, 112061. [[CrossRef](#)]
74. Asadi, A.; Arefi, H.; Fathipoor, H. Simulation of green roofs and their potential mitigating effects on the urban heat island using an artificial neural network: A case study in Austin, Texas. *Adv. Space Res.* **2020**, *66*, 1846–1862. [[CrossRef](#)]
75. Abdalla, E.M.H.; Alfredsen, K.; Muthanna, T.M. Impacts of slope and length on the hydrological performance of green roof drainage mats. *J. Hydrol.* **2024**, *632*, 130974. [[CrossRef](#)]
76. Getter, K.L.; Rowe, D.B.; Andresen, J.A. Quantifying the effect of slope on extensive green roof stormwater retention. *Ecol. Eng.* **2007**, *31*, 225–231. [[CrossRef](#)]
77. Slootweg, M.; Hu, M.; Vega, S.H.; 't Zelfde, M.v.; Leeuwen, E.v.; Tukker, A. Identifying the geographical potential of rooftop systems: Space competition and synergy. *Urban For. Urban Green.* **2023**, *79*, 127816. [[CrossRef](#)]
78. Breiman, L. Random Forests. *Mach. Learn.* **2001**, *45*, 5–32. [[CrossRef](#)]
79. López-Chacón, S.R.; Salazar, F.; Bladé, E. Hybrid physically based and machine learning model to enhance high streamflow prediction. *Hydrol. Sci. J.* **2025**, *70*, 311–333. [[CrossRef](#)]
80. Wright, M.N.; Ziegler, A. ranger: A Fast Implementation of Random Forests for High Dimensional Data in C++ and R. *J. Stat. Softw.* **2017**, *77*, 1–17. [[CrossRef](#)]
81. Altmann, A.; Tološi, L.; Sander, O.; Lengauer, T. Permutation importance: A corrected feature importance measure. *Bioinformatics* **2010**, *26*, 1340–1347. [[CrossRef](#)]
82. Molnar, C. Interpretable Machine Learning; Lulu.com. 2020. Available online: <https://christophm.github.io/interpretable-ml-book/> (accessed on 31 March 2025).
83. Apley, D.W.; Zhu, J. Visualizing the Effects of Predictor Variables in Black Box Supervised Learning Models. *J. R. Stat. Soc. Ser. B Stat. Methodol.* **2020**, *82*, 1059–1086. [[CrossRef](#)]
84. Chicco, D.; Warrens, M.J.; Jurman, G. The coefficient of determination R-squared is more informative than SMAPE, MAE, MAPE, MSE and RMSE in regression analysis evaluation. *PeerJ Comput. Sci.* **2021**, *7*, e623. [[CrossRef](#)]

85. Kafy, A.A.; Crews, K.A.; Thompson, A.E. Exploring the cooling potential of green roofs for mitigating diurnal heat island intensity by utilizing Lidar and Artificial Neural Network. *Sustain. Cities Soc.* **2024**, *116*, 105893. [[CrossRef](#)]
86. Joshi, M.Y.; Aliaga, D.G.; Teller, J.; Goodspeed, R. *Predicting Urban Heat Island Mitigation with Random Forest Regression in Belgian Cities*; Goodspeed, R., Sengupta, R., Kyttä, M., Pettit, C., Eds.; The Urban Book Series; Springer: Cham, Switzerland, 2023; pp. 305–323.
87. Bechtel, B.; Demuzere, M.; Mills, G.; Zhan, W.; Sismanidis, P.; Small, C.; Voogt, J. SUHI analysis using Local Climate Zones—A comparison of 50 cities. *Urban Clim.* **2019**, *28*, 100451. [[CrossRef](#)]
88. Ritter, A.; Muñoz-Carpena, R. Performance evaluation of hydrological models: Statistical significance for reducing subjectivity in goodness-of-fit assessments. *J. Hydrol.* **2013**, *480*, 33–45. [[CrossRef](#)]
89. Kikon, N.; Kumar, D.; Ahmed, S.A. Quantitative assessment of land surface temperature and vegetation indices on a kilometer grid scale. *Environ. Sci. Pollut. Res.* **2023**, *30*, 107236–107258. [[CrossRef](#)]
90. He, J.; Shi, Y.; Xu, L.; Lu, Z.; Feng, M.; Tang, J.; Guo, X. Exploring the scale effect of urban thermal environment through XGBoost model. *Sustain. Cities Soc.* **2024**, *114*, 105763. [[CrossRef](#)]
91. Cai, Z.; Han, G.; Chen, M. Do water bodies play an important role in the relationship between urban form and land surface temperature? *Sustain. Cities Soc.* **2018**, *39*, 487–498. [[CrossRef](#)]
92. Marzban, F.; Sodoudi, S.; Preusker, R. The influence of land-cover type on the relationship between NDVI–LST and LST–Tair. *Int. J. Remote Sens.* **2018**, *39*, 1377–1398. [[CrossRef](#)]
93. Zhang, H.; Kang, M.-Y.; Guan, Z.-R.; Zhou, R.; Zhao, A.-L.; Wu, W.-J.; Yang, H.-R. Assessing the role of urban green infrastructure in mitigating summertime Urban Heat Island (UHI) effect in metropolitan Shanghai, China. *Sustain. Cities Soc.* **2024**, *112*, 105605. [[CrossRef](#)]
94. Hidalgo García, D. Spatio-temporal analysis of the urban green infrastructure of the city of Granada (Spain) as a heat mitigation measure using high-resolution images Sentinel 3. *Urban For. Urban Green.* **2023**, *87*, 128061. [[CrossRef](#)]
95. Han, D.; An, H.; Cai, H.; Wang, F.; Xu, X.; Qiao, Z.; Jia, K.; Sun, Z.; An, Y. How do 2D/3D urban landscapes impact diurnal land surface temperature: Insights from block scale and machine learning algorithms. *Sustain. Cities Soc.* **2023**, *99*, 104933. [[CrossRef](#)]
96. Luo, P.; Yu, B.; Li, P.; Liang, P.; Zhang, Q.; Yang, L. Understanding the relationship between 2D/3D variables and land surface temperature in plain and mountainous cities: Relative importance and interaction effects. *Build. Environ.* **2023**, *245*, 110959. [[CrossRef](#)]
97. Sezer, N.; Yoonus, H.; Zhan, D.; Wang, L.; Hassan, I.G.; Rahman, M.A. Urban microclimate and building energy models: A review of the latest progress in coupling strategies. *Renew. Sustain. Energy Rev.* **2023**, *184*, 113577. [[CrossRef](#)]
98. Tsoka, S.; Tsikaloudaki, A.; Theodosiou, T. Analyzing the ENVI-met microclimate model’s performance and assessing cool materials and urban vegetation applications—A review. *Sustain. Cities Soc.* **2018**, *43*, 55–76. [[CrossRef](#)]
99. Susca, T.; Zanghirella, F.; Del Fatto, V. Building integrated vegetation effect on micro-climate conditions for urban heat island adaptation. Lesson learned from Turin and Rome case studies. *Energy Build.* **2023**, *295*, 113233. [[CrossRef](#)]
100. Cristiano, E.; Deidda, R.; Viola, F. Awareness and willingness to pay for green roofs in Mediterranean areas. *J. Environ. Manag.* **2023**, *344*, 118419. [[CrossRef](#)]
101. De Oliveira Santos, T.D.; Pacheco, F.A.L.; Fernandes, L.F.S. A systematic analysis on the efficiency and sustainability of green facades and roofs. *Sci. Total Environ.* **2024**, *932*, 173107. [[CrossRef](#)] [[PubMed](#)]
102. Senent-Aparicio, J.; López-Ballesteros, A.; Jimeno-Sáez, P.; Pérez-Sánchez, J. Recent precipitation trends in Peninsular Spain and implications for water infrastructure design. *J. Hydrol. Reg. Stud.* **2023**, *45*, 101308. [[CrossRef](#)]
103. Jia, S.; Weng, Q.; Yoo, C.; Xiao, H.; Zhong, Q. Building energy savings by green roofs and cool roofs in current and future climates. *npj Urban Sustain.* **2024**, *4*, 23. [[CrossRef](#)]
104. Rahman, M.A.; Arndt, S.; Bravo, F.; Cheung, P.K.; van Doorn, N.; Franceschi, E.; del Río, M.; Livesley, S.J.; Moser-Reischl, A.; Pattnaik, N.; et al. More than a canopy cover metric: Influence of canopy quality, water-use strategies and site climate on urban forest cooling potential. *Landsc. Urban Plan.* **2024**, *248*, 105089. [[CrossRef](#)]
105. Ibsen, P.C.; Crawford, B.R.; Corro, L.M.; Bagstad, K.J.; McNellis, B.E.; Jenerette, G.D.; Diffendorfer, J.E. Urban tree cover provides consistent mitigation of extreme heat in arid but not humid cities. *Sustain. Cities Soc.* **2024**, *113*, 105677. [[CrossRef](#)]
106. Sen, S.; Khazanovich, L. Limited application of reflective surfaces can mitigate urban heat pollution. *Nat. Commun.* **2021**, *12*, 3491. [[CrossRef](#)]

Disclaimer/Publisher’s Note: The statements, opinions and data contained in all publications are solely those of the individual author(s) and contributor(s) and not of MDPI and/or the editor(s). MDPI and/or the editor(s) disclaim responsibility for any injury to people or property resulting from any ideas, methods, instructions or products referred to in the content.